Letters

A Similarity-Based Robust Open-Circuit Fault Diagnosis Method for Dual Pulse Rectifiers

Qingli Deng, *Student Member, IEEE*, Shuai Zhao, *Member, IEEE*, Chunxu Lin, *Student Member, IEEE*, Bin Gou, *Member, IEEE*, Dong Xie, *Member, IEEE*, Xinglai Ge, *Senior Member, IEEE*, Xiaoyun Feng, and Huai Wang, *Senior Member, IEEE*

***Abstract*—This letter proposes a current similarity-based robust diagnosis scheme to detect open-circuit (OC) faults for insulated gate bipolar transistors (IGBTs) in dual pulse rectifiers. The similarity indicator between the ac-side currents of the two rectifiers is calculated based on the structural characteristics, which are independent of system parameters and naturally robust to voltage fluctuations and load changes. Also, it avoids modeling or additional sensors. Then a proper threshold is designed by analyzing variable behaviors under various normal and faulty operating conditions. Finally, the faulty switches are located by the integrals of the extracted dc-side current and designed time-sequence current indicators without injecting specific driving signals. The effectiveness of the proposed fault diagnosis method is demonstrated by both simulation and experimental testing.**

***Index Terms*—Dual pulse rectifiers, fault diagnosis, similarity indicator, threshold design.**

I. Introduction

PULSE rectifiers provide bidirectional energy conversion between ac-side and dc-side for traction converter systems in railway applications, which usually operate at a low switching frequency of 350 or 450 Hz. As a result, it has considerable ac-current harmonics. Therefore, dual pulse rectifiers, which consist of two H-bridge modules connected in parallel, are utilized to reduce the ac-side current harmonics and current stress for the switching devices [1]. Compared with the single pulse rectifier, dual pulse rectifiers have doubled the number of insulated gate bipolar transistors (IGBTs), as shown in Fig. 1, increasing the probability of open-circuit (OC) faults and posing risks to system reliability and safety.

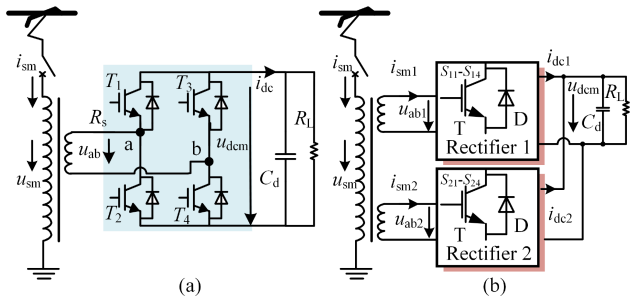

Fig. 1. Topology diagrams of (a) single pulse rectifier and (b) dual pulse rectifiers.

In the state-of-the-art research on OC fault diagnosis, signal-based, model-based, and data-driven methods have been studied. Model-based methods signify the fault occurrence by assessing residuals, which are generated by subtracting measurable signals from reference signals based on precise mathematical system models [2], [3], [4], [5]. The reference ac-side current in [2] and [3], dc-side voltage [4], and ac-side input voltage [5] are obtained by building the mixed logic dynamic model or circuit mathematical model to detect the OC faults, performing a fast diagnostic speed. However, it relies on accurate system models and threshold judgment mechanisms, making them sensitive to parameter variation and threshold level. Besides, the OC faults perform similar current signatures with the internal symmetric topology of pulse rectifiers, leading to the difficulty of locating faulty switches. Specific driving signals are injected to distinguish similar pairs of faulty switches in [2], which introduces a degree of intrusiveness to the system.

Signal-based methods extract the fault symptoms from the measurable signals, such as the current distortion-based method in [6]. It is characterized by its simplicity with the sensitivity to load variations, noise, and disturbances [7]. The data-driven methods achieve fault recognition without modeling and threshold setting, but acquiring a large amount of historical data for offline training and the online implementation of machine learning models is challenging [8].

Manuscript received 8 February 2024; revised 12 April 2024; accepted 1 May 2024. Date of publication 6 May 2024; date of current version 20 June 2024. This work was supported in part by the State Scholarship Fund of China Scholarship Council (CSC), and in part by the IEEE PELS Graduate Studies Scholarship and Jan Abraham "Braham" Ferreira Scholarship. *(Corresponding author: Bin Gou.)*

Qingli Deng, Chunxu Lin, Bin Gou, Xinglai Ge, and Xiaoyun Feng are with the Ministry of Education Key Laboratory of Magnetic Suspension Technology and Maglev Vehicle, Southwest Jiaotong University, Chengdu 610031, China (e-mail: qinglideng@my.swjtu.edu.cn; lincx@my.swjtu.edu.cn; bingo@swjtu.edu.cn; xlge@swjtu.edu.cn; fengxy@home.swjtu.edu.cn).

Shuai Zhao and Huai Wang are with the AAU Energy, Aalborg University, 9220 Aalborg, Denmark (e-mail: szh@energy.aau.dk; hwa@energy.aau.dk).

Dong Xie is with the Professorship of Power Electronics, Chemnitz University of Technology, 09126 Chemnitz, Germany (e-mail: dong.xie@etit.tu-chemnitz.de).

Color versions of one or more figures in this article are available at https://doi.org/10.1109/TPEL.2024.3397049.

Digital Object Identifier 10.1109/TPEL.2024.3397049

Regarding the fault symptoms of dual pulse rectifiers, the dc-side voltage distortion may arise from either rectifier 1 or rectifier 2, due to their parallel configuration. This issue has not been considered in the conventional voltage-based diagnosis methods (e.g., [4]), limiting its applicability in dual pulse rectifiers. Meanwhile, due to the isolation effect of the traction transformer, each rectifier can operate independently, which means the failure of one module hardly affects another. To this end, each rectifier can be diagnosed independently by the ac-side current distortion-based methods described above. However, two measurable ac-side currents from the two rectifiers exhibit similarity due to identical positions and electrical parameters, which brings a new opportunity to improve OC fault diagnosis. Based on structural characteristics, a current reference signal can be obtained, which requires no modeling efforts and is independent of system parameters.

Although the conventional current residual-based fault diagnosis strategy can be employed in dual pulse rectifiers, an appropriate threshold level setting is difficult for residual-based fault judgment mechanisms [9]. Moreover, the robustness of OC fault diagnosis for pulse rectifiers is challenged by complicated operation conditions in the practical implementation process [10]. By contrast, similarity-based fault diagnosis methods take advantage of simple threshold setting for fast speed of fault detection and high false alarm immunity, which have been verified effectively in the applications of a two-level three-phase rectifier in [11], modular multilevel converters in [12], and multisector permanent magnet synchronous motor systems in [13], for example. Inspired by the above-outlined challenges and opportunities, this letter proposes a similarity-based diagnosis method for OC faults in dual pulse rectifiers in railway applications.

The novel aspects of the proposed method are: 1) an ac-side current similarity-based indicator with a proper threshold is applied for fault detection in dual pulse rectifiers; and 2) the dc-side current and time-sequence current features are extracted and designed to locate the specific faulty rectifiers and switches. The proposed method has the following advantages: 1) it is robust because the designed diagnostic indicators are less sensitive to the traction system operation modes (e.g., traction, braking), ac-side voltage fluctuations, measurement errors, and component parameter variances; and 2) it is easy to implement without the need for additional sensors, circuit modeling, and signal injection.

II. Proposed Diagnosis Method

A. Normal Operation and Phase Alignment

As depicted in Fig. 1, two rectifier modules, denoted as rectifier 1 and rectifier 2, are connected to the secondary side of the transformer, forming a coupling at the transformer's primary side. The dynamic behavior of the system [1] can be described as

$$\begin{cases} L_{\mathrm{sj}}\frac{di_{\mathrm{smj}}}{dt} = u_{\mathrm{smj}} - R_{\mathrm{sj}}i_{\mathrm{smj}} - u_{\mathrm{abj}} \\ C_{\mathrm{d}}\frac{du_{\mathrm{dc}}}{dt} = i_{\mathrm{dcj}} - \frac{u_{\mathrm{dc}}}{R_{\mathrm{L}}} \\ i_{\mathrm{sm}} = i_{\mathrm{sm1}} + i_{\mathrm{sm2}} \end{cases} \tag{1}$$

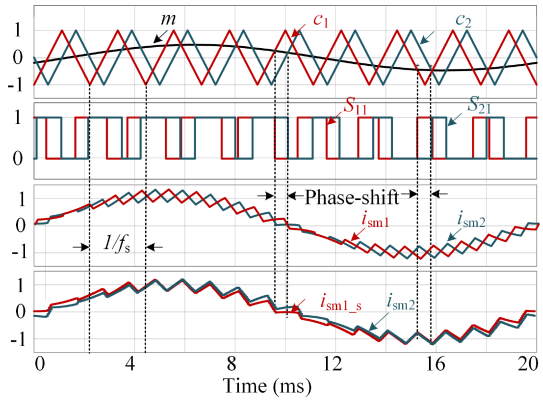

Fig. 2. Alignment process of ac-side current in dual pulse rectifiers.

where the subscript j represents the rectifier modules index. u_{smj} and i_{smj} denote the ac-side voltage and current of the transformer's secondary side, respectively. i_{sm} denotes the ac-side current of the transformer's primary side. u_{abj} represents the ac-side input voltage of the rectifiers. R_{sj} and L_{sj} denote the ac-side equivalent resistance and inductance, respectively. u_{dc} and i_{dc} represent the dc-side voltage and current. C_{d} and R_{L} denote the dc-side capacitor and the equivalent load, respectively.

Usually, a DQ coupling control strategy is employed for the dual pulse rectifiers. The control strategy involves carrier phase-shift modulation with a specific phase difference, typically set at 90°, between the two rectifiers. Given the low probability of both rectifiers occurring OC faults simultaneously, their ac-side currents can serve as reference signals for each other when aligned in phase.

To achieve the phase alignment of two currents, this process involves computing the phase difference between two signals, converting it into the corresponding discrete data calibration step, and then adjusting one of the current signals. Initially, the phase difference depends on the modulation and carrier wave phases of the two current signals. The modulation wave is primarily affected by changes in the modulation index, which are reflected in the ac-side input voltage and ac-side voltage signals of the two rectifiers. However, the effects on the two rectifiers are consistent due to the structural characteristics, thereby keeping the phase difference between two ac-side currents unchanged. As such, on the premise of equivalent circuit parameters within the two modules, their modulation wave signals can be regarded as identical. Consequently, the carrier wave phases primarily account for the phase difference between the two currents.

To visualize the phase-shift impact on the current signals, the modulation, carrier waves (denoted as m, c_1, and c_2, respectively), and pulse signals are analyzed. As presented in Fig. 2, within a switching cycle, the phase of the carrier signal transitions from 0° to 360°. Hence, a phase difference of 90° corresponds to one-fourth of a switching cycle. The discrete data calibration step can be calculated by dividing the control period, which can be expressed as

$$N_{\mathrm{c}} = \frac{1}{4}\cdot\frac{1}{f_{\mathrm{s}}}\cdot\frac{1}{T_{\mathrm{c}}} \tag{2}$$

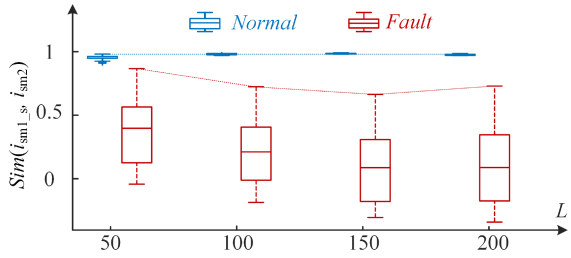

Fig. 3. Sim value scope with different data window length L.

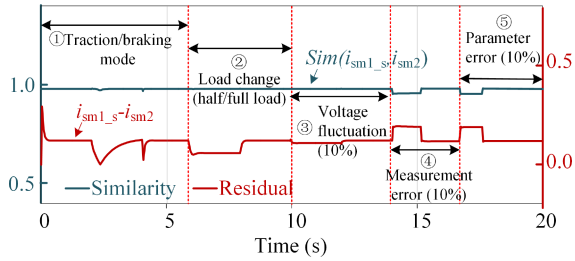

Fig. 4. Dynamic behavior of similarity and residual in simulation.

where the N_c represents the calibration step of discrete data for phase alignment, f_s is the switching frequency, and T_c is the control period.

Taking the ac-side current of rectifier 2 as the phase reference, the current phase of rectifier 1 is adjusted by N_c to obtain the phase-calibrated signal for i_{sm1}. As such, the adjusted signal i_{sm1_s} is aligned closely with i_{sm2}, ensuring both magnitude and directional variations are well-matched.

B. Fault Detection and Threshold Design

This alignment enables the similarity measurement indicator calculation, forming the basis for the fault detection system. In an applied time window, this current similarity indicator Sim is proposed as

$$Sim\left(i_{sm1\_s}, i_{sm2}\right) = \frac{\sum_{k=1}^{L} i_{sm1\_s}(k) \cdot i_{sm2}(k)}{\sqrt{\left(\sum_{k=1}^{L} i_{sm1\_s}^2(k)\right) \cdot \left(\sum_{k=1}^{L} i_{sm2}^2(k)\right)}} \tag{3}$$

where $i_{sm1\_s}(k)$ and $i_{sm2}(k)$ denote the signals i_{sm1_s} and i_{sm2} at time instance k.L represents the number of the data points, which equals the quotient of the applied time window length and the control cycle.

During the normal operation, the similarity indicator Sim tends to 1, while it decreases when an OC fault occurs. Thus, the value ranges of the Sim value under normal and fault conditions serve as the foundation for accurate detection. The time window length is crucial for extracting Sim. Shorter time window lengths are preferred for faster detection speeds. However, shorter time windows may fail to capture sufficient fault signatures, decreasing sensitivity to faults. Given that OC faults exhibit periodic characteristics within half of the fundamental cycle, the applied time window lengths for Sim extraction are set at 1/8, 1/4, 3/8, and 1/2 of the fundamental cycle, corresponding to data window lengths L of 50, 100, 150, and 200, respectively. Fig. 3 illustrates the scope of Sim values with different data window lengths L. It can be observed that normal data tend to stabilize after L exceeds 100, with a clear distinction of the Sim value between fault data and normal data. This trend remains consistent as L increases to 150 and 200. Ultimately, the data window length of 100 is selected to balance the detection time and accuracy.

The robustness of the fault detection method is important for practical application, as it depends on the selected indicators being sensitive to faults while remaining independent of other

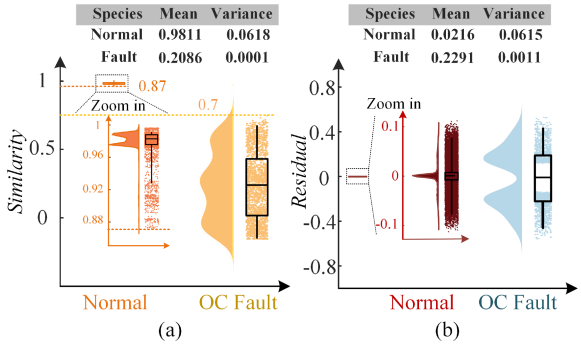

Fig. 5. Indicators data distribution, statistical mean, and variance in historical data of (a) similarity and (b) residual.

factors. As for dual pulse rectifiers in railway applications, these factors include operational modes, load variations, input voltage fluctuations, parameter variances, and measurement errors. Given this, a data-informed decision-making strategy is utilized to evaluate the behavior of the proposed similarity indicator and design a proper threshold under these conditions. A conventional residual indicator is then introduced by generating the difference between the two signals of i_{sm1_s} and i_{sm2}. Two comparative analyses are then conducted, involving dynamic behavior in simulations and statistical analysis in historical data.

The dynamic behavior of similarity and residual in the simulation test during normal operation is depicted in Fig. 4. It compares the performance of two indicators under different dynamic operation profiles without faults. As shown, the proposed indicator Sim is significantly less sensitive than the residual to the dynamic operation conditions, with a relatively consistent value of around 0.98 during traction/braking mode, full and half load changes, voltage fluctuations, measurement errors, and parameter errors.

The data distribution and statistical analysis in historical data of similarity and residual are shown in Fig. 5. The historical data cover the instances of normal and fault operation across traction/braking modes, ac-side voltage with $\pm 15\%$ fluctuations, load changes with half and full load, and parameters of $\pm 20\%$ variations. To visualize the data distribution of the Sim and residual indicators across the historical data, Fig. 5 compares their probability density plot, boxplot, scatter plot, statistical mean, and variance of the normal and faulty database. The statistical means of Sim and residual approaches 1 and 0 with similar variances of 0.0618 and 0.0615, respectively,

indicating high stability and consistency. However, the Sim performs more stable than the residual in fault data with smaller variances of 0.0001. Moreover, the Sim values exhibit a notable discrimination capability between normal and fault data, with a relatively high minimum value of 0.87 during normal operation and a maximum value of 0.7 during faults.

The comparative analysis between the two indicators highlights the advantages of the proposed similarity metric. In terms of a proper threshold setting, it is determined by minimizing the probability of normal data misjudgment and the probability of fault data misdetection in the meantime. According to the statistical analysis of historical fault data, the threshold settings between 0.7 and 0.87 all meet the requirements. This study selects a threshold of 0.7 to accommodate noise, disturbances, multiple operation modes, measurement inaccuracies, and parameter errors under normal conditions.

C. Location of Faulty Switch

Each rectifier consists of four switches, marked as T_{j1}, T_{j2}, T_{j3}, and T_{j4}. To locate the faulty modules and switches, further efforts are made by extracting the intrinsic features from analyzing the prior fault knowledge. During normal operational conditions, the rectifiers transfer the energy between the ac and dc sides with different switching modes. When an OC fault occurs, the fault switches directly block the related energy transmission path, thereby making the dc-side output current become zero. Considering the magnitude and direction of the dc-side output current can reflect the energy transmission between the ac and dc sides, the dc-side output currents of the two rectifiers are computed through the switching function model S_{abj} [3]. To enhance this feature, their integration over the applied time window is expressed as

$$E_j = \int i_{dcj} dt = \int S_{abj} \cdot i_{smj} dt \tag{4}$$

where the E_1 and E_2 represent the integration of dc-side output current i_{dc1_s} and i_{dc2}, respectively, serving as indicators for locating the faulty rectifier module.

The faulty rectifier module j exhibits an absolute value reduction in E_j when an OC fault occurs. As a result, an OC fault occurs in rectifier 1 when the absolute value of E_1 is smaller than that of E_2. To mitigate errors during the comparison process, the judgment criterion is applicable only when the relative magnitude relationship between E_1 and E_2 persists for one switching cycle.

In an OC fault event occurring in either T_{j2} or T_{j3}, it leads to distortion in the positive current waveform. In contrast, an OC fault in T_{j1} or T_{j4} results in distortion in the negative current waveform. As such, the current polarity can be utilized to locate the faulty switch pairs of T_{j2} & T_{j3} and T_{j1} & T_{j4}. However, these switch pairs are symmetrically positioned within the H-bridge topology, which poses a difficulty due to the similar fault signatures.

Specifically, the distinctive factor is that the peak moment of distorted current during a T_{j2} fault coincides with the trough moment observed during a T_{j3} fault. Also, the behaviors T_{j1} or T_{j4} are analogous. Pulse-sequence sampling is designed to extract the features of switch pairs. The OC faults in T_{j2} and T_{j3} are illustrated as an example, as shown in Fig. 6(a). When the driving signal S_{j2} shifts from 1 to 0, the peaks of distorted current associated with the T_{j3} OC fault can be captured. Conversely, the peaks of distorted current related to the T_{j2} OC fault become evident when the driving signal S_{j3} shifts from 0 to 1. An analogous analysis can be applied to the T_{j1} and T_{j4} OC faults.

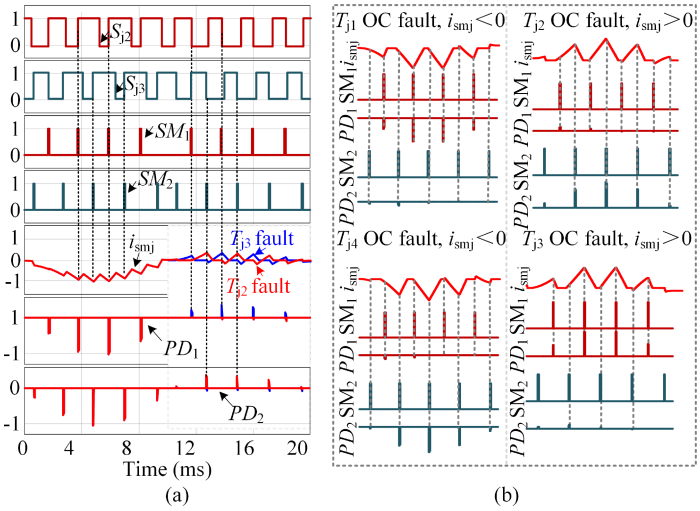

Fig. 6. Similar faults analysis. (a) Switching moments for T_{j2} and T_{j3} OC faults. (b) Pulse-sequence features for four switches.

Denoting the switching moments (SM) of the driving signals of similar fault pairs as SM_1 and SM_2, the peaks of distortion (PD) current at these moments can be calculated by multiplying SM with the ac-side current i_{smj}. Hence, the SM_1, SM_2, PD_1, and PD_2 for OC faults in similar fault pairs are pictured in Fig. 6(b), respectively. To achieve the feature enhancement (FE) for the values of PD_1 and PD_2, they are integrated within the applied time window, denoted as FE_1 and FE_2, are expressed as

$$\begin{cases} FE_1 = \int PD_1\, dt = \int i_{smj} * SM_1\, dt \\ FE_2 = \int PD_2\, dt = \int i_{smj} * SM_2\, dt. \end{cases} \tag{5}$$

With these new indicators and the relationship depicted in Fig. 6, the faulty switch can be precisely located when it satisfies one of the following principles for a switching cycle:

$$\begin{cases} FE_1 < FE_2 \& FE_2 < 0, & T_{j1} \text{ OC fault} \\ FE_1 < FE_2 \& FE_1 > 0, & T_{j2} \text{ OC fault} \\ FE_1 > FE_2 \& FE_2 > 0, & T_{j3} \text{ OC fault} \\ FE_1 > FE_2 \& FE_1 < 0, & T_{j4} \text{ OC fault.} \end{cases} \tag{6}$$

It is essential to emphasize that the previously analyzed switching moments and pulse-sequence feature extraction findings are subject to the traction operation mode. In braking conditions, similar fault pairs lead to the same current distortion, making it indistinguishable from measurement signals.

Para.	Sim.	Ex.
u_s	25000 V	50 V
f_g	50 Hz	50 Hz
n_r	25000/1550	1/1
L_{s1}/L_{s2}	5.4/5.4 mH	2/2 mH
R_s	0.2Ω	0.1 Ω
C	9 mF	2.8 mF
R_L	20 Ω	40 Ω
f_s	450 Hz	1000 Hz
T_c	50 μs	50 μs

(a)

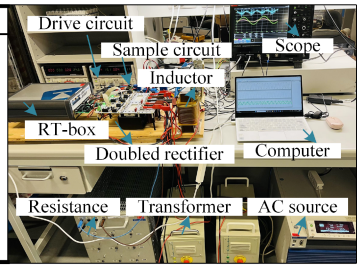

(b)

Fig. 7. Two setups of the dual pulse rectifiers with full-scale simulation and down-scale experiment. (a) Specifications and (b) down-scale prototype.

III. Case Study and Verification

Two setups of the dual pulse rectifiers with full-scale simulation (Sim.) and down-scale experiment (Ex.) are implemented to assess the effectiveness of the proposed fault diagnosis method. Test parameters setting and the down-scale prototype are detailed in Fig. 7, including the u_s, ac-side frequency f_g, transformer ratio (n_r), L_{s1}, L_{s2}, R_s, C_d, R_L, f_s, and T_c. These parameters primarily differ in terms of power levels and switching frequencies. In the full-scale simulation, a switching frequency of 450 Hz is chosen to mitigate the impact of high switching losses, aligning with industrial applications. Conversely, in the down-scale experiment, a higher switching frequency of 1000 Hz is employed to minimize the harmonic generation. These variations further facilitate the method's adaptability validation across different switching frequencies.

Scale adjustments are made to ensure the applicability of the proposed method to both full-scale and down-scale parameters before the test. Specifically, the ac-side currents are standardized by dividing their root mean square values. To enhance visualization, the ac-side voltage is adjusted to the interval $[-5, 5]$ by scaling the reference voltage levels of 500 and 10 V in full-scale and down-scale systems, respectively. Subsequently, the performance of the proposed fault detection and location method is analyzed under different operating conditions and testing scenarios.

A. Fault Detection and Module Location Under Braking Operation Mode

In the braking operation mode, the ac-side currents of two rectifiers are standardized and calibrated. As shown in Fig. 8, the similarity indicator Sim is calculated based on the aligned currents. When an OC fault occurs in rectifier 1, as depicted in Fig. 8(a), i_{sm1_s} exhibits distortion while i_{sm2} remains normal. The value of Sim begins to decrease, triggering the $Detection\_Flag1$ when it falls below the predefined threshold of 0.7. Simultaneously, the energy flowing through the modules, as represented by E_1 and E_2, undergoes significant changes due to the blockage of current flow in the faulty module. E_1 approaches 0, and E_2 continues to vary with the current. Thus, the faulty module is localized as rectifier 1, and the $Module\_Flag2$ steps to 1.

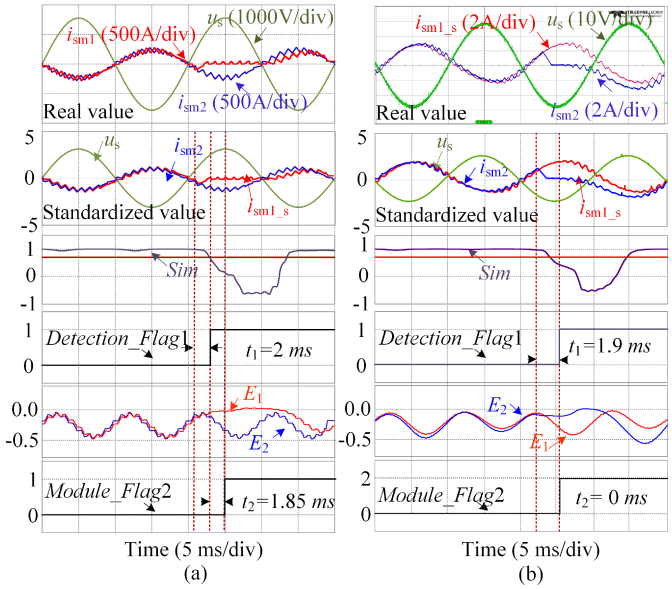

Fig. 8. Fault detection and module location tests under braking operation mode. (a) Rectifier 1 OC fault in full-scale simulation. (b) Rectifier 2 OC fault in down-scale experiment.

Similarly, the OC fault of rectifier 2 can be analyzed, as shown in Fig. 8(b). Regarding the detection time t_1 and module location time t_2, the full-scale simulations are 2 and 1.85 ms, while the down-scale experiments are 1.9 and 0 ms, respectively.

B. Fault Detection, Module, and Switch Location Under Traction Operation Mode

Under traction operation mode, where the ac-side current and voltage are in the same direction, opposite to the braking mode. The T_{22} and T_{13} OC faults are set in the full-scale simulation, while the T_{14} and T_{23} OC faults are set in the down-scale experiment, as shown in Figs. 9 and 10, respectively. The analysis process for fault detection and module location is similar to that under the braking mode. As for the switch location, the values of FE_1 and FE_2 are extracted and compared. The $Switch\_Flag$ transitioned to 2 because FE_1 is smaller than FE_2, and FE_1 is greater than 0 for one switching cycle, as depicted in Fig. 9(a). While the $Switch\_Flag$ transitioned to 3 because FE_1 is bigger than FE_2, and FE_2 is greater than 0 for one switching cycle, as depicted in Fig. 9(b). The difference between FE_1 and FE_2 is quite small since the similar feature of the switch pairs. However, a definitive relationship between them can be ensured in a switching cycle according to Fig. 6.

During down-scale experiments, additional factors such as noise interference and measurement errors are introduced into the detection and location processes. As shown in Fig. 10, the experimental results maintain diagnostic outcomes comparable to those observed in simulations, highlighting the robustness of the proposed method. This indicates its favorable adaptability across systems with varying parameters. The diagnostic time t, consisting of detection time t_1 and location time t_2, averages around 3 ms.

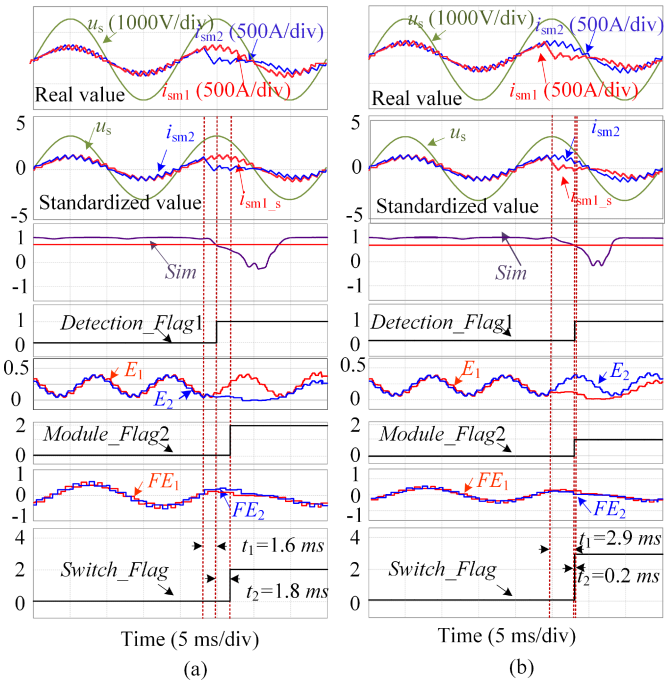

Fig. 9. Diagnostic process in traction mode of the full-scale simulation for (a) T_{22} and (b) T_{13} OC faults.

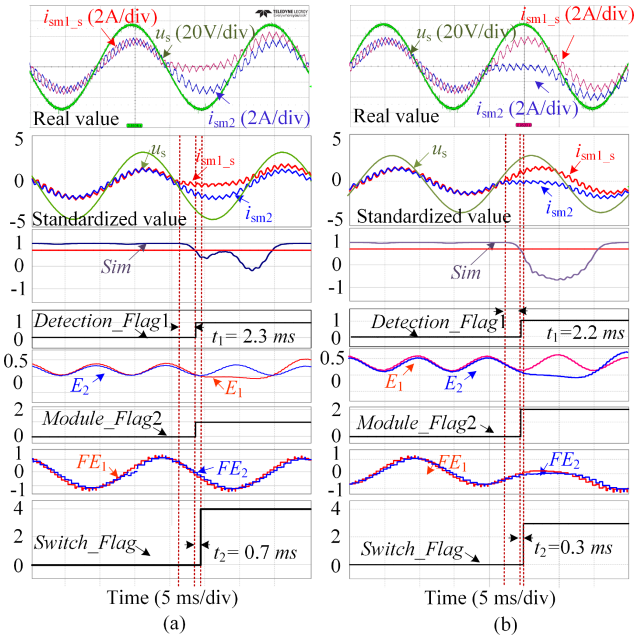

Fig. 10. Diagnostic process in traction mode of the down-scale experiment for (a) T_{14} and (b) T_{23} OC faults.

C. Robustness Validation

To further validate the robustness of the proposed method, more tests are conducted on the down-scale experimental platform under different operating conditions and scenarios. These conditions include modulation index variations with different ac-side voltages (Case1&2, Case3&4), load changes (Case1&3, Case2&4), and parameter variances (Case5&6). Eight types of OC faults randomly occurring are tested, and the detection and location results of each fault type and their average detection and location times are illustrated in Fig. 11. As shown, the solid points represent instances where the diagnostic results match the given fault types, while hollow points indicate inconsistencies. The experimental results highlight its robustness to diverse operating conditions, i.e., the operation modes, voltage fluctuation, load changes, parameter variances, and measurement errors. As a result, the proposed method achieves a diagnostic accuracy of 100% across multiple experimental tests, with an average diagnostic time of 4 ms.

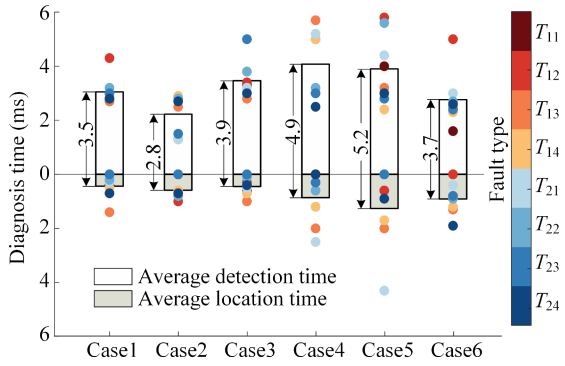

Fig. 11. Diagnostic metrics under different test conditions:
Case 1 with $u_s = 20$ V, $R_L = 80\ \Omega$, $L_{s1} = 2$ mH, $L_{s2} = 2$ mH, $C_d = 2.8$ mF.
Case 2 with $u_s = 30$ V, $R_L = 80\ \Omega$, $L_{s1} = 2$ mH, $L_{s2} = 2$ mH, $C_d = 2.8$ mF.
Case 3 with $u_s = 20$ V, $R_L = 40\ \Omega$, $L_{s1} = 2$ mH, $L_{s2} = 2$ mH, $C_d = 5$ mF.
Case 4 with $u_s = 30$ V, $R_L = 40\ \Omega$, $L_{s1} = 2$ mH, $L_{s2} = 2$ mH, $C_d = 5$ mF.
Case 5 with $u_s = 25$ V, $R_L = 40\ \Omega$, $L_{s1} = 2$ mH, $L_{s2} = 2$ mH, $C_d = 5$ mF.
Case 6 with $u_s = 30$ V, $R_L = 80\ \Omega$, $L_{s1} = 2$ mH, $L_{s2} = 1$ mH, $C_d = 2.8$ mF.

Investigations, including the performance evaluation between similarity and residual indicators, the applied time window length, and the threshold setting, are conducted to enhance the robustness of fault detection further. Both full-scale simulation and down-scale experimental tests under various dynamic operation conditions verify the effectiveness of the proposed method.

In conclusion, Figs. 8–11 showcase the consistent behavior and the mutually complementary validation between full-scale and down-scale setups, demonstrating the effectiveness of the proposed method across systems with different power levels and switching frequencies. Compared to traditional fault diagnosis approaches for the single pulse rectifier, although the diagnostic time is slightly higher than the 2–3 ms reported in [2] and [3] for residual-based fault diagnosis methods, the proposed method does not require modeling to obtain reference signals or the injection of switch signals to locate the faulty switches, which is simple and preferable for field implementation.

IV. Conclusion

A robust similarity-based fault diagnosis method is proposed for OC faults in the application of dual pulse rectifiers, which is independent of system parameters and naturally robust to voltage fluctuations and load changes. The OC faults are detected and located without the need for modeling, additional sensors, or signal injection.

REFERENCES

[1] I. A. Tasiu, Z. Liu, Q. Yan, H. Chen, K. Hu, and S. Wu, "Fuzzy observer based control for the traction dual rectifiers in high-speed train," *IEEE Trans. Veh. Technol.*, vol. 70, no. 1, pp. 303–318, Jan. 2021.

[2] B. Gou, X. Ge, S. Wang, X. Feng, J. B. Kuo, and T. G. Habetler, "An OC fault diagnosis method for single-phase PWM rectifier using a model-based approach in high-speed railway electrical traction drive system," *IEEE Trans. Power Electron.*, vol. 31, no. 5, pp. 3816–3826, May 2016.

[3] D. Xie, J. Pu, and X. Ge, "Current residual-based method for open-circuit fault diagnosis in single-phase PWM converter," *IET Power Electr.*, vol. 11, no. 14, pp. 2279–2285, Nov. 2018.

[4] J. Zhang, T. Peng, C. Yang, Z. Chen, H. Tao, and C. Yang, "A voltage-based hierarchical diagnosis approach for open-circuit fault of two-level traction converters," *Electronics*, vol. 8, no. 9, pp. 992, 2019.

[5] D. Xie, C. Lin, H. Lin, W. Liu, Y. Du, and T. Basler, "OC switch fault diagnosis, pre- and postfault DC voltage balancing control for a CHBMC using SVM concept," *IEEE Trans. Power Electron.*, vol. 39, no. 1, pp. 677–692, Jan. 2024.

[6] T. Shi, Y. He, T. Wang, J. Tong, B. Li, and F. Deng, "An improved open-switch fault diagnosis technique of a PWM voltage source rectifier based on current distortion," *IEEE Trans. Power Electron.*, vol. 34, no. 12, pp. 12212–12225, Dec. 2019.

[7] X. Ge, J. Pu, and Y. Liu, "Online OC fault diagnosis method in single-phase PWM rectifiers," *Electron. Lett.*, vol. 51, no. 23, pp. 1920–1922, Nov. 2015.

[8] Q. Deng, B. Gou, X. Ge, C. Lin, D. Xie, and X. Feng, "A high-accuracy-light-AI data-driven diagnosis method for open-circuit faults in single-phase PWM rectifiers," *IEEE Trans. Transp. Electrific.*, vol. 9, no. 3, pp. 4352–4365, Sep.. 2023.

[9] G. Conte, A. M. Perdon, and E. Zattoni, "Fault detection problems for switching linear systems: A structural approach," *IEEE Trans. Autom. Control*, vol. 68, no. 10, pp. 5890–5905, Oct. 2023.

[10] X. Li, J. Xu, Z. Chen, S. Xu, and K. Liu, "Real-time fault diagnosis of pulse rectifier in traction system based on structural model," *IEEE Trans. Intell. Transp. Syst.*, vol. 23, no. 3, pp. 2130–2143, Mar. 2022.

[11] F. Wu and J. Zhao, "Current similarity analysis-based open-circuit fault diagnosis for two-level three-phase PWM rectifier," *IEEE Trans. Power Electron.*, vol. 32, no. 5, pp. 3935–3945, May 2017.

[12] D. Zhou, H. Qiu, S. Yang, and Y. Tang, "Submodule voltage similarity-based open-circuit fault diagnosis for modular multilevel converters," *IEEE Trans. Power Electron.*, vol. 34, no. 8, pp. 8008–8016, Aug. 2019.

[13] Y. Du, C. Li, and Z. Zheng, "An online metric learning-based open-switch and current sensor fault diagnosis for MSPMSM systems," *IEEE Trans. Power Electron.*, vol. 38, no. 7, pp. 8966–8976, Jul. 2023.